# Leveraging Bayesian optimization for automated plasma composition optimization of ARC with physics-based turbulent transport models

**Audrey Saltzman**[1*], Pablo Rodriguez-Fernandez[1], Aaron Ho[1], Garud Snoep[1], Jiyun Han[1], Jo Hall[1], Marco Muraca[1], and Nathan Howard[1]

MIT Plasma Science and Fusion Center[1], audreysa@mit.edu[*] This work is supported by Commonwealth Fusion Systems under RPP020 and the National Science Foundation Graduate Research Fellowship under Grant No. 2141064.

Plasma Science & Fusion Center

Commonwealth Fusion Systems

The complex interplay of plasma composition and geometry with both pedestal pressure and turbulent transport, and the resulting impact on fusion power, make optimization with physics-based transport models a valuable endeavor. Here, we seek to maximize the fusion power of the ARC power plant [21].

## Background

Plasma composition includes the density at the pedestal boundary condition (neped), the effective charge (Zeff), main ion fraction (fmain). The impurity mix is uniquely defined by Zeff and fmain.

$$Z_{eff} = \sum \frac{n_i Z_i^2}{n_e} \qquad f_{main} = \frac{n_{DT}}{ne}$$

The first three moments of the plasma geometry are elongation (ε), triangularity (δ), and squareness (ζ). These can be defined both by the Turnbull-Miller [1] and Miller Extended Harmonic (MXH) [2] equilibria.


Figure 1: Depiction of the impact elongation, triangularity, and squareness have on the plasma (adapted from https://wiki.fusion.ciemat.es/).

Changes to plasma composition and plasma geometry impact fusion performance through changes in the turbulent transport, pedestal pressure, H-mode power threshold, and the total fusion volume.

### Impact on pedestal pressure

- Higher $\mathbf{n_{e,ped}}$**:** beneficial to pressure for peeling modes but deleterious for ballooning modes.
- Higher **zeff:** peeling ballooning transition occurs at lower $n_{e,ped}$ but peeling branch pedestal pressure increases for the same $n_{e,ped}$ [3].
- Higher **elongation:** stabilizes the ballooning branch [4].
- Higher **triangularity:** increases the peeling branch pedestal pressure for the same $n_{e,ped}$ [5].
- Lower (positive) **squareness:** increases the pedestal pressure [6].

### Impact on turbulent transport

- Higher **impurity concentration:**
  - ⇒ can stabilize the main ion ITG [8,9], experimental evidence of which is found in [10,11,12].
  - ⇒ can destabilize the impurity drift mode [13,14], the impurity ITG mode [15], and the TEM mode [16].
- Higher **elongation:** stabilizes turbulence [17].
- Higher **triangularity:** can be destabilizing at high elongation [18].
- Higher **squareness:** Mixed evidence [19,20]

### Impact on burning plasma volume

- **Squareness** can potentially be used for volumetric optimization [7].

## Methods

Integrated modeling is performed using **MAESTRO,** which combines **PORTALS-TGLF** [22,23], **EPED** [24], **TRANSP** [25], and **MEGPy** [26].

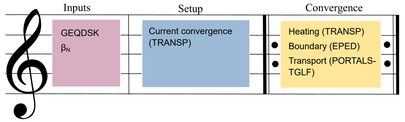


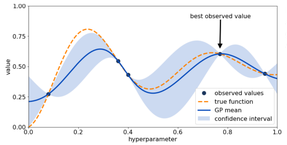


Figure 2: Process of fitting a gaussian process surrogate to observed values. Adapted from [27].

Bayesian optimization (BO) fits surrogates to data previously acquired from an expensive black box function to select the most valuable point to evaluate next.

## Uncertainty propagation

Assuming independence between sources, the total relative uncertainty on reported Pfus values is ~34%.

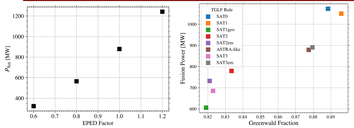


Figure 3: The stated 20% uncertainty of EPED results in a relative std of $\sigma_{Pfus}$ =15%.

Figure 4: Variation in TGLF saturation rule results in a wide range of fusion power, with a relative std of $\sigma_{Pfus}$ =15%, when considering SAT1geo, SAT2, SAT2em, SAT3, SAT3em.

## Brute force scans

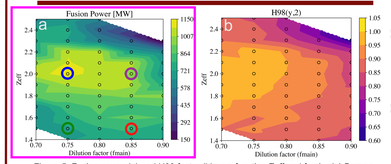


Figure 5: Fusion power (a) and H98 factor (b) as a function Zeff and fmain. (a) Demonstrates fusion power can be increased by moving to a higher impurity concentration operating point. The nominal operation point is circled in red. (b) Demonstrates the importance of using physics-based models, instead of empirical, to capture these effects.

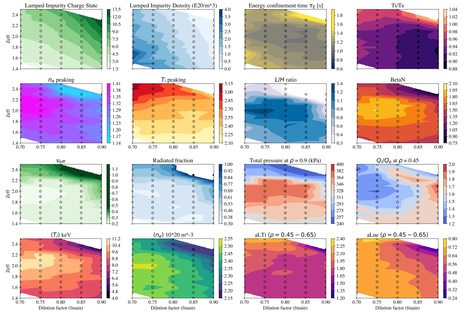


Figure 6: Additional quantities plotted from the same scan depicted in Figure 8. The charge of the lumped impurity increasing with increase Zeff and fmain. Both density and temperature peaking increase with more impurities. The operating point with the highest fusion power is well above the L-H transition power threshold.

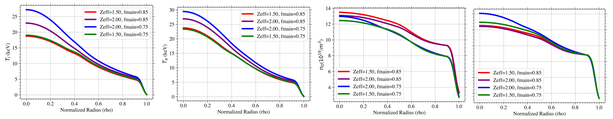


Figure 7: Profiles at the locations circled in corresponding colors in figure 8a. Adding impurities stabilizes turbulence resulting in higher temperature and density peaking. However, they reduce the concentration of fuel ions.

Adding impurities can increase the expected fusion power generated by ARC.

## Standalone 1D scans

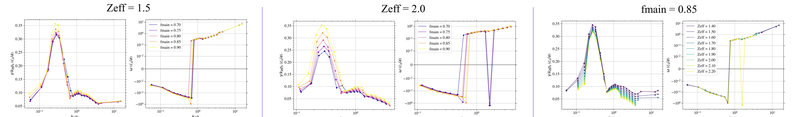


Figure 8: Stand alone TGLF scans on the output from the nominal ARC case MAESTRO simulation. Decreasing the main ion fraction is much more stabilizing when at high values of Zeff. Increasing Zeff is stabilizing. These results are consistent with the shape of the plot in Figure 8a.

Changes in main ion fraction have different effects on the turbulence at different values of Zeff.

Plasma geometry and composition both have strong impacts on the predicted pedestal performance.

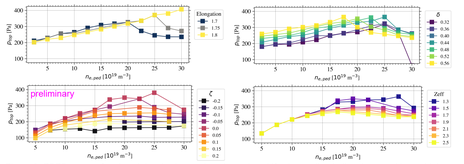


Figure 9: EPED scans of pedestal density. Increasing elongation shifts the pealing-ballooning transition to higher densities. Increasing triangularity has the opposite effect and additionally shifts the pealing branch to higher pressures. Negative squareness might degrade the pedestal pressure. Higher Zeff shifts the peeling-ballooning transition to lower densities and reduces the pressure in the ballooning branch.

## Bayesian Optimization

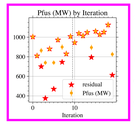


Figure 10: Inputs and resulting performance as a function of iteration. The lines on the plots below show the value of inputs that has led to the best fusion power, enforcing the constraint fLH > 1 and fG <1, so far. To the left of the dotted grey line demarcates training data.

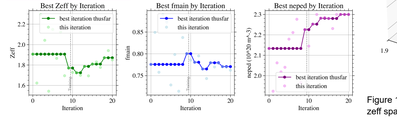


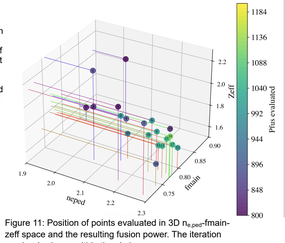


Figure 11: Position of points evaluated in 3D $n_{e,ped}$-fmain-zeff space and the resulting fusion power. The iteration number is shown within the circle.

Bayesian optimization allows us to find the optimum considering three input dimensions, zeff and fmain as in the brute force scan, with the addition of $n_{e,ped}$.

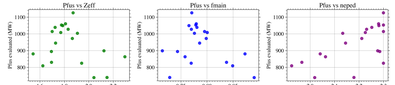


Figure 12: 1D plots demonstrating the trend in performance between each input and the resulting fusion power. The scatter demonstrates the interconnections between the inputs and results.

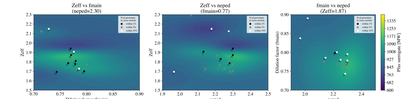


Figure 13: 2D cross sections of the surrogate models taken at the location of the best MAESTRO evaluation. The dots show evaluations the surrogate was trained on; the color represents how close the evaluation was to the cross section value.

## Conclusions

I. Through optimization of impurities in ARC, the **fusion power can be increased by ~30%**. More impurities are also more favorable to core-edge integration.

II. **Uncertainty** on fusion power predictions is driven both by uncertainty about turbulent transport and by uncertainty in the pedestal boundary condition.

III. **Physics-based transport models**, rather than empirical scaling laws, are required to capture the full impact of impurities and shaping.

IV. There is a **complex relationship between changing Zeff + fmain** (or equivalently the lumped impurity charge + concentration) and the resulting change in fusion power (see Rodriguez-Fernandez in session JO04).

V. Increasing impurities results in improved performance predominately by increasing temperature and density peaking, which can overcome the deleterious effects of reducing the concentration of the fuel ions.

VI. **BO allows efficient exploration** of more operating parameters.

## Future Work

- Explore the impacts of changing plasma geometry, in addition to plasma composition, on the full integrated model predictions.
- Perform BO in **all six dimensions** ($n_{e,ped}$, Zeff, fmain, elongation, triangularity, squareness).

## References

[1] Turnbull PoP 1999
[2] Arbon PPCF 2022
[3] Hall APS DPP 2025
[4] Kim PoP 2022
[5] Urano NF 2014
[6] Leonard NF 2007
[7] Parisi Phys. Rev. Res. 2025
[8] Migliuolo NF 1992
[9] Rodriguez-Fernandez PoP 2024
[10] McKee PRL 2000
[11] Boedo NF 2000
[12] Lazarus J Nucl. Mat. 1984
[13] Han NF 2025
[14] Dong & Horton PoP 1995
[15] Frojdh Chalmers Thesis 1993
[16] Dominguez & Staebler NF 1993
[17] Angelino PRF 2009
[18] Belli PoP 2008
[19] Joiner & Dorland PoP 2010
[20] Holcomb PoP 2009
[21] Hillesheim JPP submitted 2025
[22] Rodriguez-Fernandez NF 2024
[23] Staebler NF 2021
[24] Snyder NF 2011
[25] Pankin Comput. Phys. Commun. 2025
[26] Snoep PoP 2023
[27] https://medium.com/aimonks/bayesian-optimization-revolutionizing-efficient-search-in-complex-spaces-3e2cc476d2cd